Speckle-beam oriented schlieren technique

Yusuke Nakamura, Takumi Suzuki, Kiyoshi Kinefuchi, and Akihiro Sasoh

Department of Aerospace Engineering, Nagoya University, Furo-cho, Chikusa, Nagoya 474-8603, Japan

E-mail: yusuke.nakamura@mae.nagoya-u.ac.jp

Received xxxxxx
Accepted for publication xxxxxx
Published xxxxxx

Abstract

An advanced background-oriented schlieren (BOS) method, named as the speckle-beam oriented schlieren technique, was newly developed to measure the distribution of refraction angles in transparent media. A speckle pattern is generated by passing a coherent laser beam through a holographic diffuser, a pinhole, and a lens, generating a collimated background image that is projected directly onto the image sensors. Because the intensity of the background image is maintained at a high level, this method is, in principle, useful for diagnosing fast and/or low signal-to-noise phenomena, such as high-temperature gasses with radiation emission. Moreover, by splitting the background beam into two imaging paths with different focal lengths, the refraction angles can be measured for a schlieren object with uncertain location, and the depth position of the refraction angles can be resolved. This technique was demonstrated by measuring the refraction angle and the depth position distribution in a sonic jet with different injected locations.

Graphical abstract

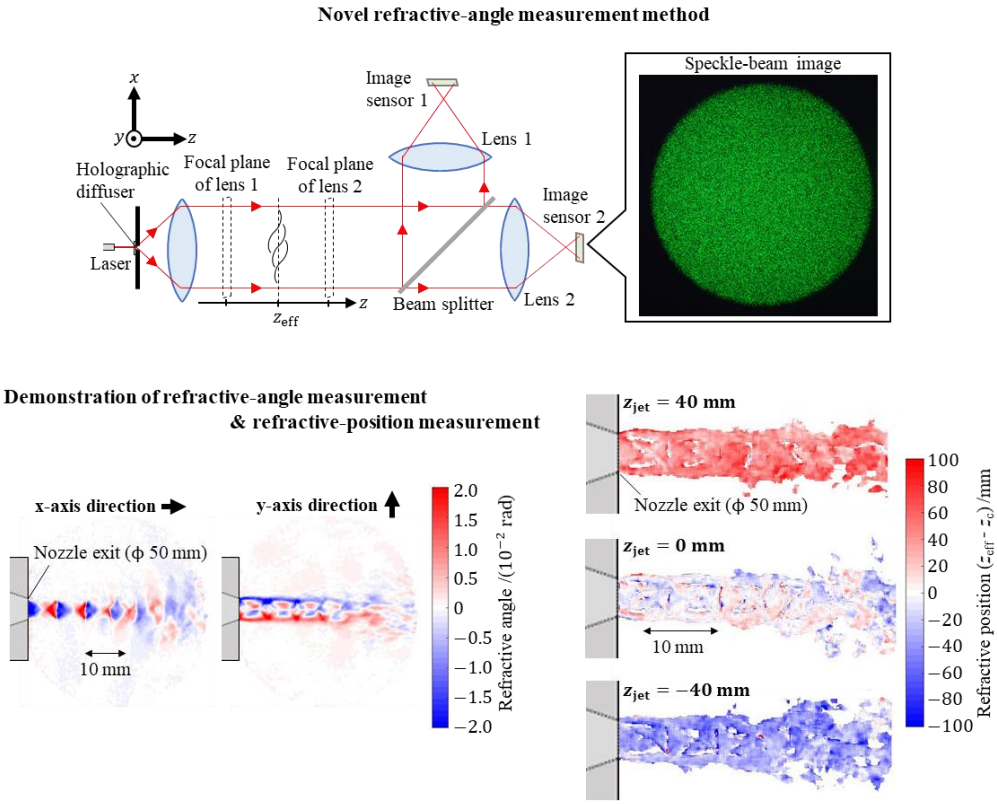

Keywords: background-oriented schlieren, schlieren imaging, depth estimation

---

Nomenclature

f	Function
f_{even}, f_{odd}	Even/odd number component of f
f_{L}	Focal length of lens L
G	Gladstone–Dale constant
$I_{i,j}$	Image
$\hat{I}_{i,j}$	Zero-mean normalized image
I_{L1}, I_{L2}	Images by L_1 and L_2
I_{raw}	Raw image
i, j	Pixel position on image plane
$i_{\mathrm{L1},0}$, $j_{\mathrm{L1},0}$	Reference position for image by L_1
$i_{\mathrm{L2},0}$, $j_{\mathrm{L2},0}$	Reference position for image by L_2
i_{M}, j_{M}	Matched position
i_{sub}, j_{sub}	Sub-pixel estimated position
i_{T}, j_{T}	Template originated position
L_1, L_2	Lens
l_{pix}	Length corresponding to one pixel
$R_{i,j}$	Cross-correlation
$T_{m,n}$	Template image
n_0	Reference refractive-index
m, n	Pixel position on template image
S_{T}	Template size
$\boldsymbol{u}_{\mathrm{L1}}$, $\boldsymbol{v}_{\mathrm{L1}}$	Vectors for correcting image by L_1

$\boldsymbol{u}_{\mathrm{L2}}, \boldsymbol{v}_{\mathrm{L2}}$	Vectors for correcting image by L_2
x, y, z	Coordinates
z_{c}	Correction parameter
z_{eff}	Effective refracted position
z_{jet}	Jet injected position
z_{r}	Position of refraction
z_{s}	Center position of schlieren object
Δz	Distance between two focal planes
$\boldsymbol{\delta}$	Displacement
$\boldsymbol{\delta}_1, \boldsymbol{\delta}_2$	Displacement at focal plane of L_1, L_2
δ_1, δ_2	Displacement defined as Equation (7)
$\boldsymbol{\delta}_{1,\mathrm{r}}, \boldsymbol{\delta}_{2,\mathrm{r}}$	Displacement by refraction
$\boldsymbol{\delta}_{\mathrm{err}}$	Error at displacement
$\boldsymbol{\varepsilon}$	Refractive angle
$\boldsymbol{\varepsilon}_{\mathrm{ray}}$	Angle of light ray
λ	Wavelength
ρ	Density

1. Introduction

Schlieren imaging is a technique employed for the visualization of density gradients in fluid using the refraction of light, which originated in the 17th century (Settles 2001). The schematic of a typical setup for schlieren imaging is illustrated in Fig. 1 (a). Light emitted from a small illuminator is collimated at the lens on the light source side and refocused by the other lens placed on the other side across a schlieren object under study. On this side, a sharp knife edge is placed at the focal point, and an image sensor is placed behind it. By this method, a simple optical system obtains the distribution of the density gradient as a luminance distribution. However, the determination of precise quantitative values by this method is difficult in comparison to laser interferometry. In recent years, numerous quantitative imaging methods avoiding the use of complex systems such as interferometry have risen in popularity owing to the development of image sensors and image processing techniques (Settles and Hargather 2017). These methods yield distributions of refractive angles. The relation between the refractive angle $\boldsymbol{\varepsilon}$ and the density ρ of the schlieren object is described as follows, using the Gladstone–Dale constant G and a reference refractive-index n_0 (Fomin 1998).

$$\boldsymbol{\varepsilon} = \frac{G}{n_0}\int \begin{pmatrix}\partial_x \\ \partial_y\end{pmatrix} \rho dz \tag{1}$$

This equation yields the density distribution, assuming a distribution along the direction of sight z or measured with the observations from different angles. The most popular among such methods is the background oriented schlieren (BOS) (Dalziel et al. 2000; Venkatakrishnan and Meier 2004; Raffel 2015). A schematic illustrating this method is shown in Fig. 1 (b). A lens and an image sensor are placed such that the background patterns printed on a screen or other materials is in the sharp focus on the image sensor. The angle of the refraction at the schlieren object placed between the background pattern and the lens is derived from the displacement of the pattern on the image sensor. An improved version of BOS using laser speckle illumination to project the pattern on the screen was also proposed (Meier and Roesgen 2013). Laser speckle photography, shown in Fig. 1 (c), is likewise popular as the quantitative measurement of refractive angles (Kihm 1997; Kawahashi and Hirahara 2000). A coherent laser beam, expanded by a lens pair comprising a concave and a convex lens, is brought to the schlieren object, and another lens and ground glass are placed on the opposite side such that the image of the schlieren object appears on the ground glass. A lens and an image sensor are placed such that the focus plane of the image is at some distance from the ground glass, and the refractive angle of each light lay is derived from a displacement of the speckle pattern on the image sensor. The information regarding where the refraction occurs in the sight direction cannot be obtained with the methods explained above. To obtain the refraction location, focusing schlieren (Weinstein 2010) and plenoptic BOS (Klemkowsky et al. 2017) methods were introduced. A schematic of the focusing schlieren method is shown in Fig. 1 (d). The source grid placed just after the Fresnel lens produces light that is equivalent to light radiated from many point-light-sources. The cutoff grid, working as a knife edge for light from each point-light-source, is placed at the position at which an image of the source grid is projected. Because the light is not collimated, the depth of focus is small. Therefore, the schlieren image is generated only by the refraction around a specific focal plane, determined by the optical setup. This method is not applicable if the location in the sight direction of refraction is not known. In contrast, with the plenoptic BOS, which is a variant of BOS using the plenoptic camera as shown in Fig. 1 (e), the refraction around an arbitral plane in the sight direction is obtained from a single image. However, this method has the disadvantage that the pixel number of the perspective image used for the displacement analysis is reduced by one-order in comparison to the raw image when the image is resampled from the hexagonal micro-lens configuration to a rectangular arrangement.

This study proposes a novel refractive-angle measurement method that can be used for observations of rapid processes or phenomena with strong light emission. This method was named speckle-beam oriented schlieren (SBOS). Moreover, we construct an improved method, which can be used for a schlieren object with uncertain location of refraction and enable determination of the location in three-dimensions. This method was named dual-focus SBOS (DF-SBOS).

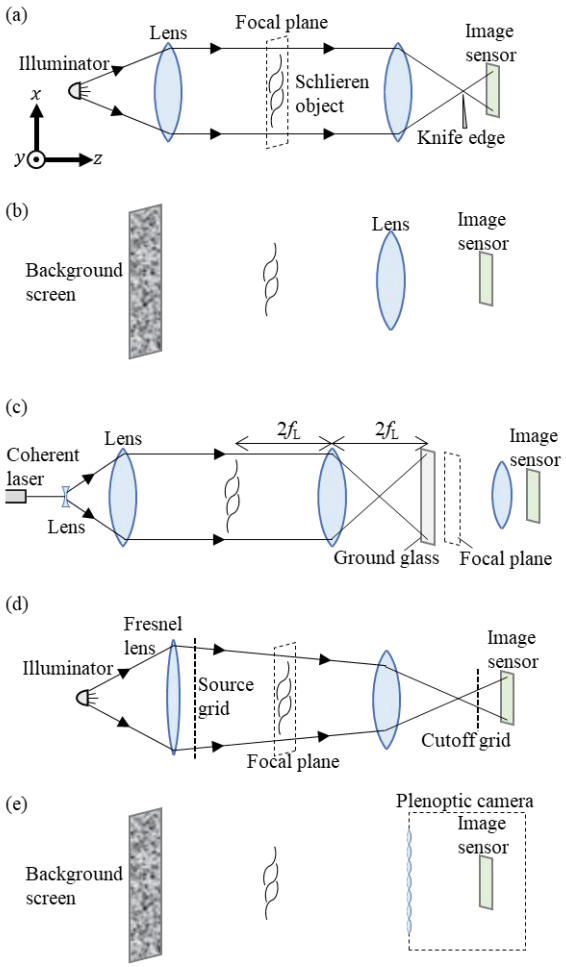

Fig. 1. Schematics of typical setups for (a) schlieren imaging, (b) background-oriented schlieren, (c) laser speckle photography, (d) focusing schlieren, and (e) plenoptic BOS.

2. Speckle-beam oriented schlieren (SBOS)

SBOS is useful for the observation of the density gradient distribution in very fast processes, which require strong reference light because the laser beam enters directly into the image sensor with little power loss. While in regular BOS, most of the light is scattered at the background screen, even if the screen was illuminated by a strong light source. In combination with a band pass filter, this method can be used for phenomena with strong light emission, such as chemical reactions or spark discharge.

2.1 Speckle-beam generation method

The key of the measurement method proposed in this study, SBOS, is a collimated laser beam projecting a speckle pattern, which we refer to as the speckle beam. The schematic image of the method employed to generate the speckle beam is shown in Fig. 2. A pinhole covered with a holographic diffuser is placed just after the coherent laser, and a lens is placed such that its focal point is exactly at the pinhole. The speckle pattern forms at the diffuser, which provides strong beam intensity, and the diffused beam passing through the pinhole is collimated at the lens. The pattern of the speckle beam remains sharp, such that the same speckle pattern is maintained at any cross-section along the beam path.

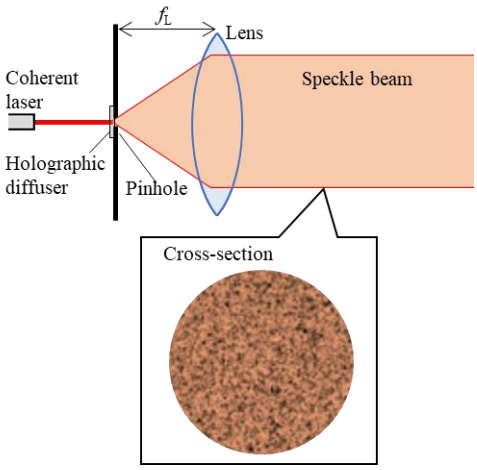

Fig. 2. Optical diagram of speckle-beam generation and speckle-beam cross-section image.

2.2 Measurement principle

The basic principle of SBOS is the same as that of BOS. The speckle-beam pattern is employed as a background pattern instead of the pattern projected on a screen or other material in the BOS. A schematic of the SBOS method is illustrated in Fig. 3. A lens pair and an image sensor are placed in the beam path, such that its focus plane is at location at an appropriate distance from the schlieren object under study. The apparent displacement $\boldsymbol{\delta}$ of the spot is measured by comparing the image captured with the schlieren object with a reference image captured without the object. The relationship between the displacement and refractive angle $\boldsymbol{\varepsilon}$, which is described as Equation (1), is expressed as follows.

$$\boldsymbol{\delta} = -\boldsymbol{\varepsilon} z_{\mathrm{r}} \tag{2}$$

Therein, z_{r} is the distance from the focal plane to the schlieren object. This equation is almost the same equation as that of BOS while z_{r} in the equation of BOS is the distance from the screen to the schlieren object. The refractive angle $\boldsymbol{\varepsilon}$ is obtained from the measured displacement $\boldsymbol{\delta}$ using this equation. For smaller z_{r}, the displacement becomes smaller, whereas the focus on the object becomes sharper. Therefore, the optimum location of the focal plane is at the position where both an appropriate displacement and sufficient spatial resolution can be obtained. The location of the focal plane can be modified by changing the lens and the image sensor positions, whereas in the BOS, the location of the screen must also be changed accordingly.

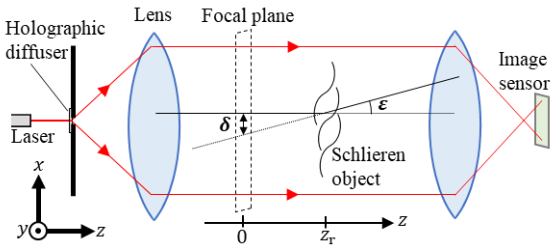

Fig. 3. Schematic of speckle-beam oriented schlieren (SBOS).

3. Dual-focus SBOS (DF-SBOS)

The other novel method, dual-focus SBOS (DF-SBOS), can be used for a schlieren object with uncertain location of refraction and enable determination of the location in three-dimensions at higher resolution.

3.1 Refractive angle measurement principle

Equation 2 is applicable only in the case where the beam is refracted within a small area around the known position z_{r}. In a more general expression, the displacement $\boldsymbol{\delta}$ can be expressed as follows.

$$\boldsymbol{\delta} = -\int_{-\infty}^{\infty} \frac{\partial \boldsymbol{\varepsilon}_{\mathrm{ray}}}{\partial z} z dz \tag{3}$$

Therein, z and $\boldsymbol{\varepsilon}_{\mathrm{ray}}$ are a position on the coordinate axis with the origin located at the focal plane and an angle of the light ray at the position z. In this equation, the position z is in the integrand. Therefore, it is difficult to obtain the refraction angle when the width of the schlieren object or the uncertainness of the location is not sufficiently small compared to the distance between the object and the focal plane. Even though this problem can be solved with the focal plane at a distance sufficiently far from the schlieren object, it leads to poor spatial resolution. Here, we introduce a refraction-angle measurement method that is applicable to the case of a schlieren object with a large width or with uncertainty of its location. A schematic of this method is illustrated in Fig. 4. The method is differentiated from SBOS in that the beam is split into two, and each beam passes through a different lens with a different focal plane. The displacements in each image with lens 1 and lens 2 can be written as follows, using a coordinate system with the origin located at the focal plane of lens 1.

$$\begin{aligned} \boldsymbol{\delta}_1 &= -\int_{-\infty}^{\infty} \frac{\partial \boldsymbol{\varepsilon}_{\mathrm{ray}}}{\partial z} z dz \\ \boldsymbol{\delta}_2 &= -\int_{-\infty}^{\infty} \frac{\partial \boldsymbol{\varepsilon}_{\mathrm{ray}}}{\partial z} (z - \Delta z) dz \end{aligned} \tag{4}$$

Therein, Δz denotes the distance between the focal planes of the two lenses. Subtracting $\boldsymbol{\delta}_2$ from $\boldsymbol{\delta}_2$, z can be omitted from the integrand.

$$\boldsymbol{\delta}_2 - \boldsymbol{\delta}_1 = \int_{-\infty}^{\infty} \frac{\partial \boldsymbol{\varepsilon}_{\mathrm{ray}}}{\partial z} \Delta z dz = \boldsymbol{\varepsilon} \Delta z \tag{5}$$

The refractive angle $\boldsymbol{\varepsilon}$ can be obtained from this equation regardless of the width or location of the schlieren object. It can be used for a schlieren object anywhere on the speckle beam path before the beam splitter, and it is not necessary that the object is between the two focal planes.

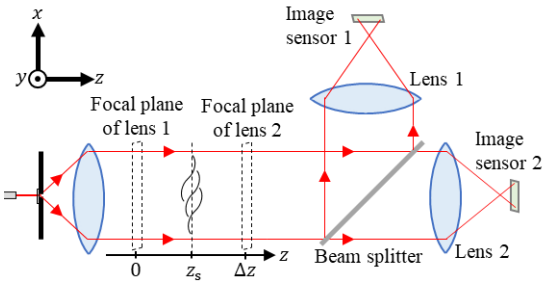

Fig. 4. Schematic of dual-focus speckle-beam oriented schlieren.

3.2 Principle of location measurement

With DF-SBOS, the location of refraction can be determined when the schlieren object is sufficiently small. The displacement δ_1 in the refraction direction can be written as follows, assuming the effective position z_{eff} of the refraction.

$$\delta_1 = -\int_{-\infty}^{\infty} \left(\frac{\partial \boldsymbol{\varepsilon}_{\mathrm{ray}}}{\partial z} \cdot \frac{\boldsymbol{\varepsilon}}{|\boldsymbol{\varepsilon}|} \right) z dz \equiv -|\boldsymbol{\varepsilon}| z_{\mathrm{eff}} \tag{6}$$

$$\delta_1 \equiv \boldsymbol{\delta}_1 \cdot \frac{\boldsymbol{\varepsilon}}{|\boldsymbol{\varepsilon}|} = \frac{\boldsymbol{\delta}_1 \cdot (\boldsymbol{\delta}_2 - \boldsymbol{\delta}_1)}{|\boldsymbol{\delta}_2 - \boldsymbol{\delta}_1|} \tag{7}$$

The effective position z_{eff} can be obtained from measured displacements using the following equation, derived from Equation (5) and Equation (6).

$$\frac{-\delta_1}{|\boldsymbol{\delta}_2 - \boldsymbol{\delta}_1|} = \frac{z_{\mathrm{eff}}}{\Delta z} \tag{8}$$

The geometrical meaning of z_{eff} is illustrated in Fig. 5. z_{eff} represents the intersection of the extended line of the initial ray of light and the extended line of the ray after refraction. z_{eff} is not always identical to the location of the refraction in the case where the schlieren object exhibits some distribution along the sight direction. The difference of these is discussed in the following. The function f around the center position z_{s} of the schlieren object is defined as follows and it is divided into the components of an even function f_{even} and an odd function f_{odd}.

$$\begin{aligned} \frac{\partial \boldsymbol{\varepsilon}_{\mathrm{ray}}}{\partial z} \cdot \frac{\boldsymbol{\varepsilon}}{|\boldsymbol{\varepsilon}|} &\equiv f(z - z_{\mathrm{s}}) \\ &= f_{\mathrm{even}}(z - z_{\mathrm{s}}) + f_{\mathrm{odd}}(z - z_{\mathrm{s}}) \end{aligned} \tag{9}$$

$$f_{\mathrm{even}}(z - z_{\mathrm{s}}) \equiv \frac{1}{2}\big(f(z - z_{\mathrm{s}}) + f(-z + z_{\mathrm{s}})\big) \qquad f_{\mathrm{odd}}(z - z_{\mathrm{s}}) \equiv \frac{1}{2}\big(f(z - z_{\mathrm{s}}) - f(-z + z_{\mathrm{s}})\big)$$

Then, Equation (8) is rewritten as follows.

$$\begin{aligned} \frac{-\delta_1}{|\boldsymbol{\delta}_2 - \boldsymbol{\delta}_1|} &= \frac{\int_{-\infty}^{\infty} \left(\frac{\partial \boldsymbol{\varepsilon}_{\mathrm{ray}}}{\partial z} \cdot \frac{\boldsymbol{\varepsilon}}{|\boldsymbol{\varepsilon}|}\right) z dz}{\Delta z |\boldsymbol{\varepsilon}|} \\ &= \frac{\int_{-\infty}^{\infty} f(z - z_{\mathrm{s}}) z dz}{\Delta z \int_{-\infty}^{\infty} f(z - z_{\mathrm{s}}) dz} \\ &= \frac{z_{\mathrm{s}}}{\Delta z} + \frac{\int_{-\infty}^{\infty} f(z) z dz}{\Delta z \int_{-\infty}^{\infty} f(z) dz} \\ &= \frac{z_{\mathrm{s}}}{\Delta z} + \frac{\int_{-\infty}^{\infty} f_{\mathrm{odd}}(z) z dz}{\Delta z \int_{-\infty}^{\infty} f_{\mathrm{even}}(z) dz} \end{aligned} \tag{10}$$

This equation shows that the effective position z_{eff} is identical to the position z_{s} of the schlieren object when the odd function component is negligibly small compared to that of the even function. Hence, the symmetric center of the schlieren object is given by Equation (8). The more accurate position of the center can be obtained for a larger absolute integral value of the even function component, which is equal to the magnitude $|\boldsymbol{\varepsilon}|$ of the refractive angle.

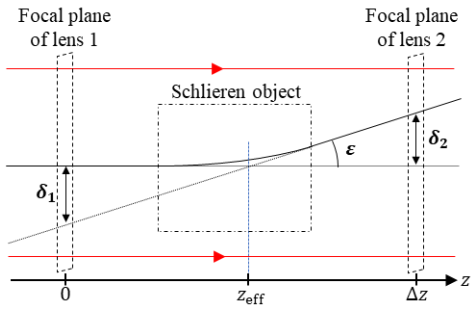

Fig. 5. Geometrical meaning of each parameters in DF-SBOS

4. Experiment

4.1 Experimental setup

Experiments were conducted using an air jet to demonstrate the SBOS and DF-SBOS methods. The schematic of these experiments is illustrated in Fig. 6. A diode pumped solid state laser (MGL-H-532, Changchun New Industries Optoelectronics Technology Co.) with a wavelength of 532 nm was used as the laser source, and the speckle beam was generated via a holographic diffuser (#55-440, Edmond Optics) with a diffusion angle of 60° and an achromatic lens whose focal length and diameter are 100 mm and 50 mm, respectively. Because the diameter of the diffused beam was greater than that of the lens, the speckle-beam diameter corresponded to that of the lens at 50 mm. A beam splitter and mirrors were placed as shown in Fig. 6, and two achromatic lenses (L_1, L_2) were placed on each split beam pass. The focal lengths of lens L_1 and lens L_2 were 300 mm and 200 mm, respectively. The beams were projected onto a MOS image sensor of a digital camera (DMC-G8, Panasonic), side by side. The size of the image sensor was 4592 × 3448 pixels. This optical system was adjusted such that the diameters of the two beams are the same, at approximately 8 mm on the image sensor. The measured distance Δz between the focus planes of two lenses was 2.7×10^2 mm. An image of the speckle pattern is shown in Fig. 7. The size of one spot in the speckle pattern is approximately eight pixels, whose equivalent length at the examined area is ~0.2 mm. SBOS is demonstrated by analyzing one of the speckle-beam images, and DF-SBOS is demonstrated by analyzing both. An air jet used for the demonstration in this study was generated by a convergent nozzle with an exit diameter of 5 mm, connected to a high-pressure chamber. The initial pressure in the chamber was set at 0.4 MPa for all experiments. A detailed explanation of this jet generator is not given in this paper, as the objective of this study is only to demonstrate the measurement methods. Details on a similar generator can be found in Kuwabara et al. (2020). The image was captured by irradiation of the image sensor with a pulsed beam of 50 μs pulsed length and long exposure time (0.5 s). The pulsed beam was triggered by the drop of the signal from the pressure sensor in the high-pressure chamber.

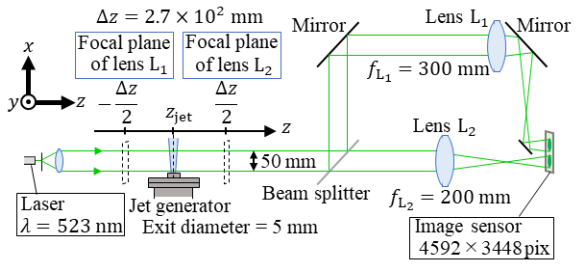

Fig. 6. Schematic of experimental setup for SBOS/DF-SBOS demonstration.

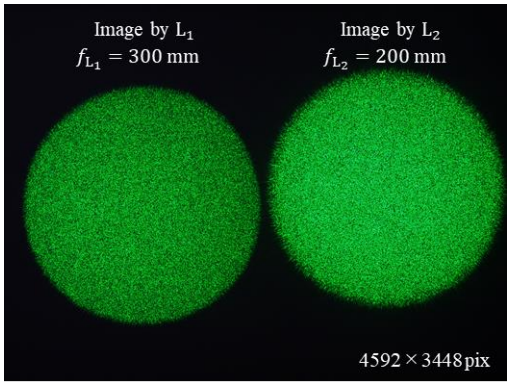

Fig. 7. Speckle-beam images obtained by two lenses on the image sensor.

4.2 Image processing

The captured speckle beams were rotated and distorted while passing through the optical elements. The extent of the rotation and distortion were different in the two beams from different lenses. An image was captured placing a transparent plate, on which a checkered pattern was printed, in the middle of the two focal planes to correct these and identify the positions on the inspection area corresponding to an arbitrary position on the image. Each side of the square on the checkered pattern is 10 mm. The image is shown in Fig. 8 (a). A point $(i_{L1,0}\, j_{L1,0})$ on the beam image with lens L_1, which corresponds to another point $(i_{L2,0}\, j_{L2,0})$ on the beam image with lens L_2 was specified. The corrected images for each beam, which are denoted by I_{L1} and I_{L2}, were generated from the raw image I_{raw} using a vector along each side of the square on each beam image, $(\boldsymbol{u}_{L1}, \boldsymbol{v}_{L1})$ and $(\boldsymbol{u}_{L2}, \boldsymbol{v}_{L2})$.

$$I_{\mathrm{L1}}(i,j) = I_{\mathrm{raw}}(i_{\mathrm{L1}}, j_{\mathrm{L1}})$$
$$\begin{pmatrix} i_{\mathrm{L1}} \\ j_{\mathrm{L1}} \end{pmatrix} \equiv \begin{pmatrix} i_{\mathrm{L1},0} \\ j_{\mathrm{L1},0} \end{pmatrix} + \frac{\boldsymbol{u}_{\mathrm{L1}} i + \boldsymbol{v}_{\mathrm{L1}} j}{|\boldsymbol{u}_{\mathrm{L1}}|} \tag{11}$$

$$I_{\mathrm{L2}}(i,j) = I_{\mathrm{raw}}(i_{\mathrm{L2}}, j_{\mathrm{L2}})$$
$$\begin{pmatrix} i_{\mathrm{L2}} \\ j_{\mathrm{L2}} \end{pmatrix} \equiv \begin{pmatrix} i_{\mathrm{L2},0} \\ j_{\mathrm{L2},0} \end{pmatrix} + \frac{\boldsymbol{u}_{\mathrm{L2}} i + \boldsymbol{v}_{\mathrm{L2}} j}{|\boldsymbol{u}_{\mathrm{L1}}|} \tag{12}$$

The images of the checkered patterns corrected by these equations are shown in Figs. 8 (b) and (c).

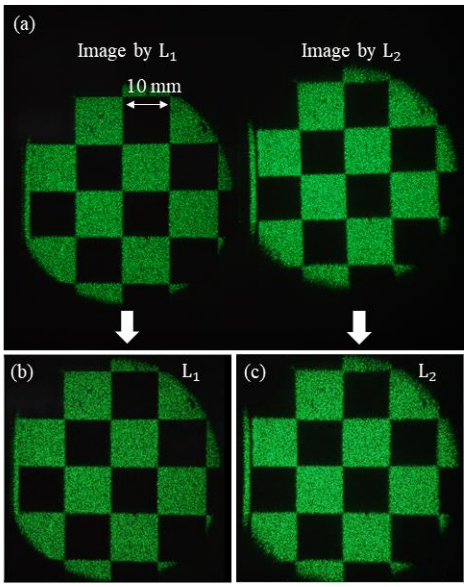

Fig. 8. Checkered pattern image. (a) Raw image. (b), (c) Corrected images.

The displacements were obtained by comparing the images acquired with and without a jet. The template image $T_{m,n}$, whose size S_{T} was 32 × 32 pixels, was cut from the image captured without a jet, and the same area matched well with the template was searched in the image with a jet, as presented below. The match was evaluated with the zero-mean normalized cross-correlation $R_{i,j}$ (Di Stefano et al. 2005), which is defined as follows.

$$R_{i,j} \equiv \frac{\sum_{m,n}\left(\hat{I}_{i+m,j+n} \cdot \hat{T}_{m,n}\right)}{\sqrt{\sum_{m,n} \hat{I}_{i+m,j+n}{}^2 \cdot \sum_{m,n} \hat{T}_{m,n}{}^2}} \tag{13}$$

$$\hat{I}_{i+m,j+n} \equiv I_{i+m,j+n} - \frac{\sum_{m,n} I_{i+m,j+n}}{S_{\mathrm{T}}}$$
$$\hat{T}_{m,n} \equiv T_{m,n} - \frac{\sum_{m,n} T_{m,n}}{S_{\mathrm{T}}} \tag{14}$$

The cross-correlation was calculated for each position $(i\ j)$ around the point $(i_{\mathrm{T}}\ j_{\mathrm{T}})$ at which the template was originated, and the matched position $(i_{\mathrm{M}}\ j_{\mathrm{M}})$ at which the cross-correlation was closest to one was determined. The resolution of the displacement obtained with this process is limited to one pixel. The sub-pixel displacement estimation (Noback and Hokanen 2005) can be obtained by the following equations.

$$i_{\mathrm{sub}} \equiv i_{\mathrm{M}} + \frac{\ln \dfrac{R_{i_{\mathrm{M}}-1,j_{\mathrm{M}}}}{R_{i_{\mathrm{M}}+1,j_{\mathrm{M}}}}}{2\ln \dfrac{R_{i_{\mathrm{M}}+1,j_{\mathrm{M}}} + R_{i_{\mathrm{M}}-1,j_{\mathrm{M}}}}{R_{i_{\mathrm{M}},j_{\mathrm{M}}}{}^{2}}}$$

$$j_{\mathrm{sub}} \equiv j_{\mathrm{M}} + \frac{\ln \dfrac{R_{i_{\mathrm{M}},j_{\mathrm{M}}-1}}{R_{i_{\mathrm{M}},j_{\mathrm{M}}+1}}}{2\ln \dfrac{R_{i_{\mathrm{M}},j_{\mathrm{M}}+1} + R_{i_{\mathrm{M}},j_{\mathrm{M}}-1}}{R_{i_{\mathrm{M}},j_{\mathrm{M}}}{}^{2}}} \tag{15}$$

The displacement $\boldsymbol{\delta}$ at the focal plane was obtained from the following equation.

$$\boldsymbol{\delta} = l_{\mathrm{pix}} \begin{pmatrix} i_{\mathrm{sub}} - i_{\mathrm{T}} \\ j_{\mathrm{sub}} - j_{\mathrm{T}} \end{pmatrix} \tag{16}$$

Therein, l_{pix} denotes the length corresponding to one pixel, where that length measured with the checkered pattern in Fig. 8 (a) was 2.2×10^{-2} mm.

4.3 Refractive angle measurement

The jet was injected perpendicular to the beam direction, and the resulting refraction was measured. Figs. 9 (a) and (b) show the displacement maps of images I_{L1} and I_{L2}, respectively, for the jet placed in the middle of the two focal planes. These are the displacements obtained with SBOS using Equation (16). Fig. 9 (c) shows the difference between those two maps, which represents the DF-SBOS result. The jet was injected from left to right in these figures. As seen in Figs. 9 (a) and (b), shock diamonds were successfully visualized in the supersonic flow around the nozzle exit. Some displacement is found throughout the area even without the jet in Figs. 9 (a) and (b), while such displacement is canceled in Fig. 9 (c). This is considered to be due to the error caused by the slight deviation of the laser beam source resulting from vibrations, etc. This error is canceled in DF-SBOS, as the magnitude of the error is the same in both displacement maps. Therefore, DF-SBOS can be considered robust to such error varying from moment to moment because of taking difference between two displacements taken at the same time. DF-SBOS was demonstrated for the jet with different exhaust positions z_{jet}, which were –40, –20, 0, 20, and 40 mm on the coordinate system, whose origin is in the middle of the two focal planes. The refractive-angle maps, which were obtained from these demonstrations are shown in Fig. 10. There are no large differences between these refractive-angle maps, which suggests that the refractive angle was successfully measured with DF-SBOS, irrespective of the placement of the jet.

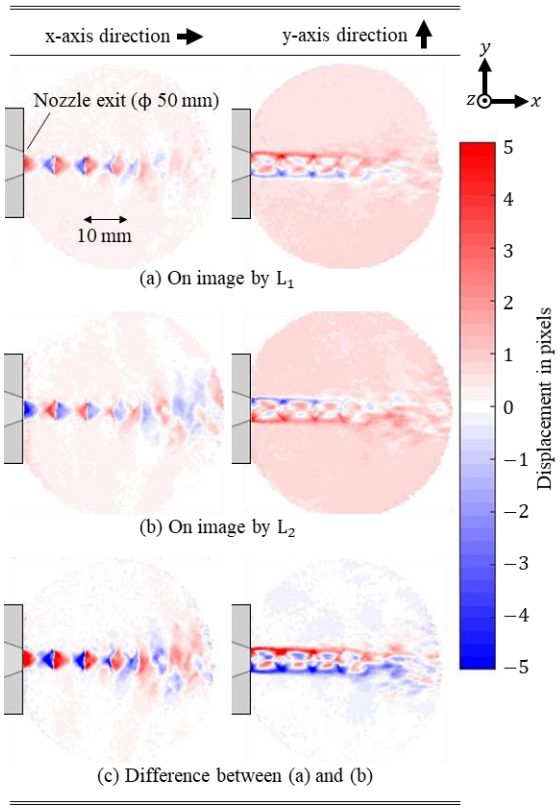

Fig. 9. Displacements of the speckle pattern to x-axis direction (left figure) and y-axis direction (right figure) on the image sensor.

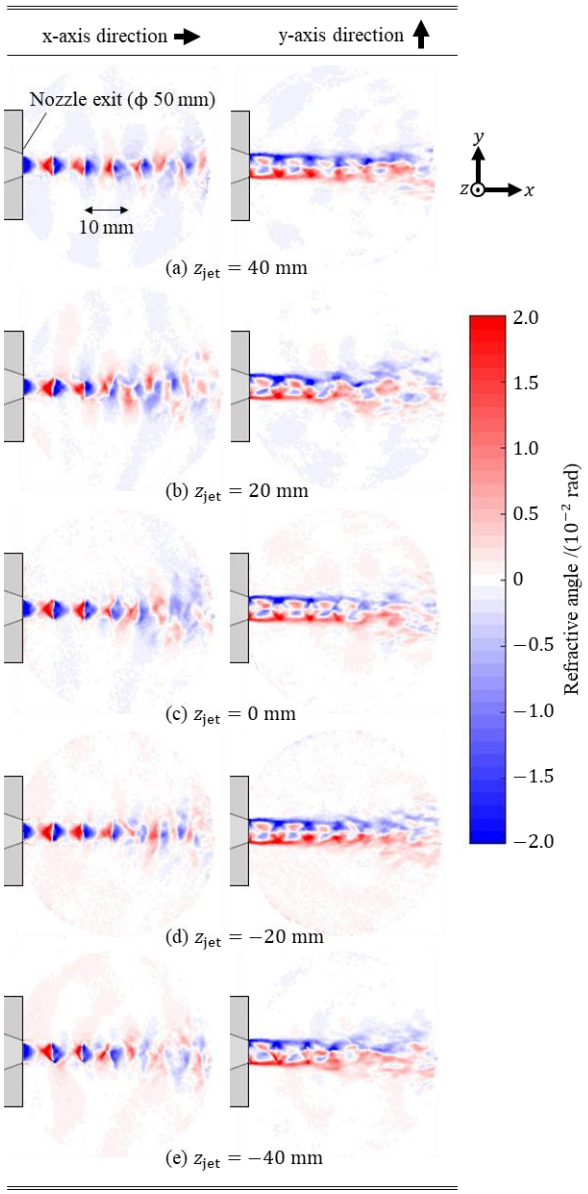

Fig. 10. Distribution of the refractive angle to x-axis direction (left figure) and y-axis direction (right figure) measured for the jet injected at each position.

4.4 Refracted position measurement

The refracted position measurement was conducted in the experiments described in Section 4.3. Even though the position can be obtained by Equation (8), the error in the resulting value without any correction is thought to be significant owing to beam deviation, which is not canceled in Equation (8). The displacement can be divided into the displacements with refraction, denoted by $\boldsymbol{\delta}_{1,\mathrm{r}}$ and $\boldsymbol{\delta}_{2,\mathrm{r}}$, and the error $\boldsymbol{\delta}_{\mathrm{err}}$, as follows.

$$\begin{aligned} \boldsymbol{\delta}_1 &= \boldsymbol{\delta}_{1,\mathrm{r}} + \boldsymbol{\delta}_{\mathrm{err}} \\ \boldsymbol{\delta}_2 &= \boldsymbol{\delta}_{2,\mathrm{r}} + \boldsymbol{\delta}_{\mathrm{err}} \end{aligned} \tag{17}$$

The displacement due to the refraction at each focal plane is of opposite signs, as each focal plane was arranged at different sides across the jet. In this case, both $\boldsymbol{\delta}_{1,\mathrm{r}}$ and $\boldsymbol{\delta}_{2,\mathrm{r}}$ are zero at the point where the difference between $\boldsymbol{\delta}_1$ and $\boldsymbol{\delta}_2$ is zero.

Therefore, the error $\boldsymbol{\delta}_{\mathrm{err}} = (\delta_{\mathrm{x,err}}\ \delta_{\mathrm{y,err}})$ is given by the following equation using $\boldsymbol{\delta}_1 = (\delta_{\mathrm{x},1}\ \delta_{\mathrm{y},1})$ and $\boldsymbol{\delta}_2 = (\delta_{\mathrm{x},2}\ \delta_{\mathrm{y},2})$ at this location.

$$\delta_{\mathrm{x,err}} = \left[\frac{\delta_{\mathrm{x},1} + \delta_{\mathrm{x},2}}{2}\right]_{\delta_{\mathrm{x},2}-\delta_{\mathrm{x},1}\cong 0}$$
$$\delta_{\mathrm{y,err}} = \left[\frac{\delta_{\mathrm{y},1} + \delta_{\mathrm{y},2}}{2}\right]_{\delta_{\mathrm{y},2}-\delta_{\mathrm{y},1}\cong 0} \tag{18}$$

Using the values obtained from these equations, Equation (8) was rewritten as follows.

$$z_{\mathrm{eff}} = \frac{(\boldsymbol{\delta}_1 - \boldsymbol{\delta}_{\mathrm{err}}) \cdot (\boldsymbol{\delta}_1 - \boldsymbol{\delta}_2)}{|\boldsymbol{\delta}_2 - \boldsymbol{\delta}_1|^2}\Delta z - \frac{\Delta z}{2} \tag{19}$$

Here, the effective refracted position was redefined in the coordinate system, whose origin is in the middle of the two focal planes. The distribution of the refracted positions z_{eff} obtained from this equation for the jet injected in the middle of the two focal planes is shown in Fig. 11. Therein, only the values in the jet element with relatively large refraction angles are displayed. The green line indicates the refractive position averaged on the line perpendicular to the jet direction (y-axis direction) at each displacement in the jet direction (x-axis direction). The position z_{eff} at each point is expected to be close to zero, as the jet is in the middle, which is not the case. This is because the positions of focal planes differ depending on the location in the beam due to lens distortion and error in alignment. Therefore, corrections are needed for more accurate measurement. In this case, the correction was made assuming that there is no difference in the distance between the two focal planes, regardless of the location in the beam. The correction parameter at each position in the x-axis direction was determined assuming that the parameter is constant along the y-axis. This assumption can be applied for the jet because the jet is sufficiently thin while the parameter difference in y-axis direction should be considered for wider jets.

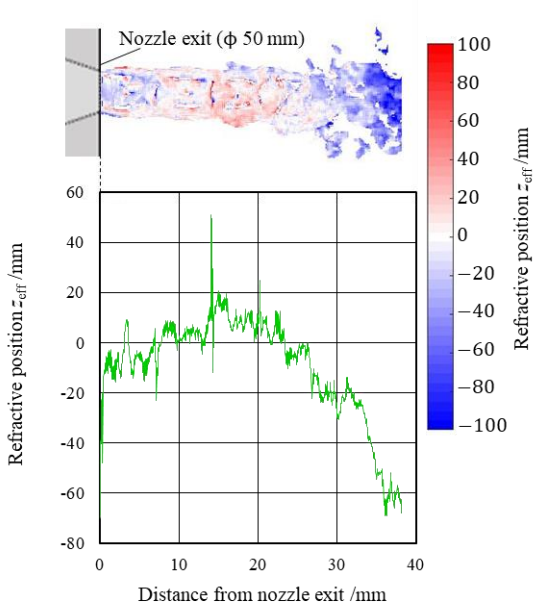

Fig. 11. Distribution of refracted positions obtained by Eq. (19) and the average with respect to the distance from nozzle exit.

Fig. 12 shows the average of five experiments with the same conditions as in Fig. 11, and the quadratic fitting curve was used as the correction parameter $z_{\mathrm{c}}(x)$. A corrected refractive position was obtained subtracting z_{c} from z_{eff}. The refracted positions were measured for the jet exhaust at the positions of –40, –20, 0, 20, and 40 mm on the z-axis using those parameters. The results are shown in Fig. 13. Fig. 14 shows the average of the measured refracted positions in all areas of the jet. The error

bars depict the standard deviation of the five experiments. The level of noise due to the error in the displacement measurement shown in Fig. 13 spans a few tens of millimeters. The resolution of the displacement measurement is approximately 0.1 pixels, which is ~10% of the displacement magnitude. The resulting noise is approximately 10% of $\Delta z = 2.7 \times 10^2$ mm, and it can be eliminated by averaging. By calculating the average of all areas of the jet, as shown in Figure 14, the error decreased to approximately 5 mm. This result demonstrates that the DF-SBOS can determine uncertain location of refraction with small error and simple setup.

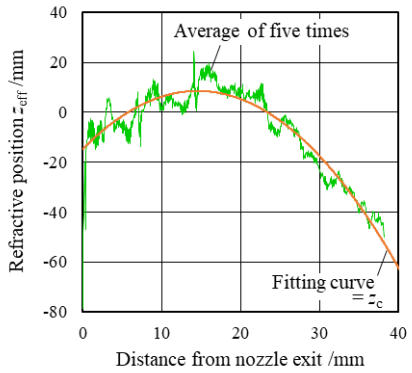

Fig. 12. Measured refracted position and fitted curve used to determine correction parameters.

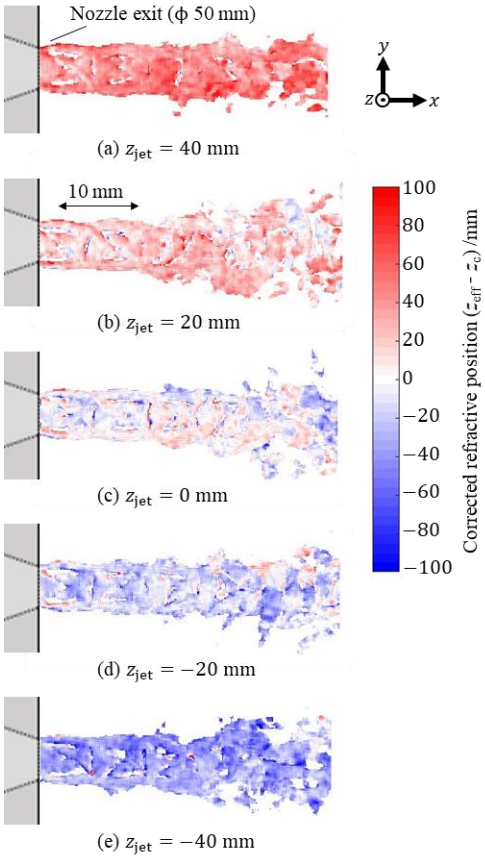

Fig. 13. Distribution of refracted positions measured for the jet injected at each position.

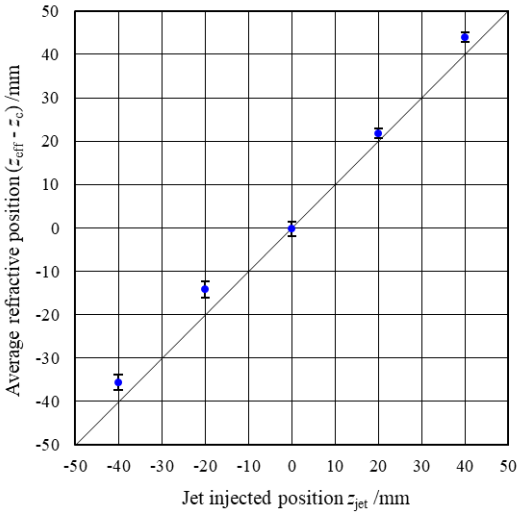

Fig. 14. Average of the refracted positions of all jet areas. Error bars depict the standard deviation of five experiments at each injected position.

5. Conclusion

A novel refractive-angle measurement method, named the speckle-beam oriented schlieren (SBOS), is proposed in this paper. The method is useful for investigating phenomena that require strong reference light for observation. A variant of this method, called the dual-focus speckle-beam oriented schlieren (DF-SBOS), is also proposed, which can be used for a schlieren object with uncertain location of refraction. We demonstrated the successful measurement of the refraction angle at the schlieren object at an unknown position, as well as the position of refraction, using an air jet. The proposed methods have potential applications both in laboratory and industrial settings, where they can be employed, for example, to find the position of a gas leak.

Declarations

Funding This work was supported by JSPS Grant-in-Aid for Scientific Research: Grant No. 18H03813

Conflicts of interest/Competing interests: We have no conflict of interest.
Availability of data and material: The datasets analyzed during this study available from the corresponding author on reasonable request.
Code availability: The codes used during this study available from the corresponding author on reasonable request.

References

Dalziel SB, Hughes GO, Sutherland BR (2000) Whole-field interaction measurements by ‘synthetic schlieren.’ Exp Fluids 28:322–335.

Di Stefano L, Mattoccia S, Tombari F (2005) ZNCC-based template matching using bounded partial correlation. Pattern Recognit Lett 26(14):2129–2134. https://doi.org/10.1016/j.patrec.2005.03.022

Fomin NA (1998) Speckle Photography for Fluid Mechanics Measurements. Springer Berlin Heidelberg. https://doi.org/10.1007/978-3-662-03707-2

Kawahashi M, Hirahara H (2000) Velocity and density field measurements by digital speckle method. Opt Laser Technol 32(7–8):575–582. https://doi.org/10.1016/S0030-3992(00)00089-X

Kihim KD (1997) Laser Speckle Photography Technique Applied for Heat and Mass Transfer Problems. Advances in Heat Transfer 30:409-439. https://doi.org/10.1017/cbo9780511575013.019
Klemkowsky JN, Fahringer TW, Clifford CJ, Bathel BF, Thurow BS (2017) Plenoptic background oriented schlieren imaging. Meas Sci Technol. https://doi.org/10.1088/1361-6501/aa7f3d
Kuwabara D, Kawasaki H, Iwakawa A, Sasoh A, Yamashita T, Taguchi K (2020) In-tube shock wave compression by piston effect of unsteady jet. Mech Eng J. https://doi.org/10.1299/mej.19-00534
Meier AH, Roesgen T (2013) Improved background oriented schlieren imaging using laser speckle illumination. Exp Fluids. https://doi.org/10.1007/s00348-013-1549-8
Nobach H, Honkanen M (2005) Two-dimensional Gaussian regression for sub-pixel displacement estimation in particle image velocimetry or particle position estimation in particle tracking velocimetry. Exp Fluids 38(4):511–515. https://doi.org/10.1007/s00348-005-0942-3
Raffel M (2015) Background-oriented schlieren (BOS) techniques. Exp Fluids 56(3):1–17. https://doi.org/10.1007/s00348-015-1927-5
Settles GS (2001) Schlieren and Shadowgraph Techniques. Springer Berlin Heidelberg. https://doi.org/10.1007/978-3-642-56640-0
Settles GS, Hargather M J (2017) A review of recent developments in schlieren and shadowgraph techniques. Meas Sci Technol 28(4):aa5748. https://doi.org/10.1088/1361-6501/aa5748
Venkatakrishnan L, Meier GEA (2004). Density measurements using the Background Oriented Schlieren technique. Exp Fluids 37(2):237–247. https://doi.org/10.1007/s00348-004-0807-1
Weinstein LM (2010) Review and update of lens and grid schlieren and motion camera schlieren. Eur Phys J Spec Top 182(1):65–95. https://doi.org/10.1140/epjst/e2010-01226-y